

Improvement in Mechanical Properties and Wear Resistance of 13Cr–4Ni Martensitic Steel by Cyclic Heat Treatment

Jai Singh¹ · S. K. Nath²

Received: 20 April 2020 / Accepted: 14 July 2020 / Published online: 14 August 2020
© The Indian Institute of Metals - IIM 2020

Abstract 13Cr–4Ni martensitic stainless steel was subjected to a cyclic heat treatment (CHT) by using Gleeble 3800, thermo-mechanical simulator. A single cycle of this heat treatment consisted of austenitization at 1000 °C, holding for 5 min and fast cooling to room temperature. The effects on microstructure and mechanical properties were studied after conducting two (1000-2c) and four such cycles (1000-4c). The wear behavior of the cyclic heat-treated and the as-received material was then investigated by conducting dry sliding wear tests on a pin-on-disk wear testing machine. The evolved microstructure after CHT consisted of a reduced fraction of undesiring δ -ferrite and retained austenite phases and thereby an increased fraction of martensitic. Along with this, refinement in the martensite blocks attributed the increased hardness (by 46%) and ultimate tensile strength (by 41%) with a slight loss of ductility. The wear resistance of cyclic heat-treated specimens was found to be 41%, 18%, and 19% higher at 10 N, 20 N, and 30 N loads, respectively, than the counterpart of the as-received specimen. The plowing and craters were found responsible for the material removal from the surface of both as-received and cyclic heat-treated specimens.

Keywords 13Cr–4Ni martensitic stainless steel · Cyclic heat treatment · Microstructure · Hardness · Wear

1 Introduction

13-4 martensitic stainless steel (13-4 MSS) possesses a good combination of corrosion resistance and mechanical strength which attracts wide applications in hydro and oil industries [1]. In these applications, the parts are required to have excellent tribological and wear properties because the failure can cause a large efficiency and economic losses. The erosive wear is more frequent in these applications which include silt erosion and cavitation erosion. But due to dynamic contact between the mating parts, some parts may degrade by sliding wear. This condition may be worsened by the vibrations caused due to the erosive wear. Both the sliding and the erosive wear are primarily influenced by surface/bulk properties. So, sliding wear resistance can be a preliminary approximation of wear and tribological characteristics of the material. A large number of studies reported the wear behavior of 13-4 MSS [2, 3]. Many techniques have been employed to enhance the surface/bulk properties of 13-4 MSS in order to enhance the wear resistance. These techniques include heat treatments (HT) [4–8], nitriding [1, 2], carburizing [9], friction stir processing [10], thermo-mechanical processing [11, 12], and coatings [13–15].

The studies based on heat treatments of 13-4 steel mainly perform the conventional heat treatments including quenching and tempering (Q&T) [4–6], double tempering [7], and intercritical tempering [8]. Amarendra et al. performed different heat treatments on 13-4 MSS to improve the mechanical properties and slurry erosion resistance [4].

✉ S. K. Nath
indiafmet@iitr.ac.in

Jai Singh
jsingh@nt.iitr.ac.in

¹ Centre of Nanotechnology, IIT Roorkee, Roorkee, UK 247667, India

² Department of Metallurgical and Materials Engineering, IIT Roorkee, Roorkee, UK 247667, India

They observed an increase in toughness, but the tensile strength and hardness decreased. Various compositions of 13-4 MSS were treated by Q&T treatment, and the effect was observed on mechanical behavior, viz. impact resistance, hardness, and tensile properties [5]. This treatment increased the ductility, but the tensile strength declined. Other researchers performed different Q&T parameters and improved the impact toughness, but the tensile strength got reduced [6]. Various parameters of double-tempering treatment were studied and compared for the hardness and the tensile properties [7] of 13-4 MSS. The intercritical tempering to improve the tensile strength of 13-4 MSS was performed and analyzed for different parameters [8]. The conventional heat treatments performed in the literature have improved one property at the expense of the other. Moreover, these treatments are time-taking techniques. So, there is need to further explore the HT techniques in order to fulfill this gap and consequently enhance the wear resistance.

In recent years, cyclic heat treatment (CHT) has added an alternate dimension in strengthening the steels. The cyclic heat treatment has been applied on various plain [16, 17] and austenitic stainless steels [18] to refine the grains and improve the mechanical properties. The present work, for the first time, conducted the cyclic heat treatments on 13-4 MSS. It is an attempt to improve the mechanical properties and consequently increase the wear resistance of 13-4 MSS. After conducting CHT on 13-4 MSS, the effects were observed after 2 and 4 cycles. The wear behavior was investigated by conducting the sliding wear tests on as-received and cyclic heat-treated specimens. Scanning electron microscopy was employed to analyze the worn surfaces and elucidate the wear mechanisms.

2 Materials and Experimental Details

13%Cr–4%Ni martensitic stainless steel (13-4 MSS) having ASTM nomenclature-ASTM A743 CA-6NM was selected in this study. The billets of 13-4 MSS were provided by Bharat Heavy Electricals Limited Haridwar, India, for research purpose. The chemical composition of the as-received (ASR) steel was examined with Thermo Jarrell Ash Spark Emission Spectroscope. The ASR steel was comprised of 0.07% C, 13.51% Cr, 3.35% Ni, 0.62% Mn, 0.64% Si, 0.32% Mo, 0.02% S, 0.01% P, 0.06% Cu, and rest Fe.

From the billets, 30-mm-long cylindrical specimens having a diameter of 10 mm were prepared for conducting cyclic heat treatment (CHT). The said treatment was performed on thermomechanical simulator, Gleeble® 3800. Figure 1 depicts the details of cyclic heat treatment (having

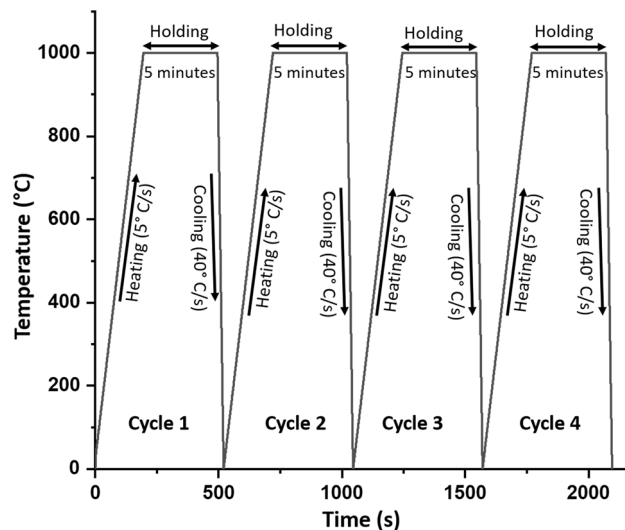


Fig. 1 The schematic procedure and parameters of cyclic heat treatment having 4 number of cycles (1000-4c)

4 number of cycles) on the temperature–time plot. The temperature of CHT was selected as 1000 °C which falls in a fully austenitic region as can be seen from Fig. 2. The phase diagram in Fig. 2 was calculated using TCFE9 (Steels/Fe-Alloys v9.0) database in Thermo-Calc software. This treatment was performed on as-received 13-4 MSS (13-4 ASR) for 2 and 4 cycles. All the characterization and the wear tests were conducted on 13-4 ASR and cyclic heat-treated specimens. The specimen taken out from

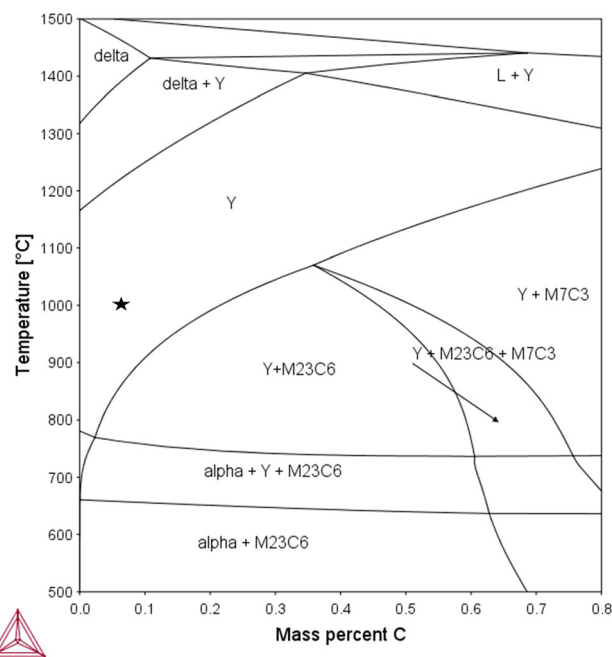


Fig. 2 Phase diagram calculated using Thermo-Calc software illustrating the temperature of (star mark) CHT (in the figure, L is liquid, and Y is austenite)

Gleeble[®] 3800 after conducting 2 cycles is designated as 1000-2c and 4 cycles as 1000-4c. Various other parameters of CHT have been studied in our other studies.

The microstructure of as-received and processed steel was examined by following the standard metallographic techniques. Small specimens were cut and polished with emery papers of 320, 800, 1200, and 1500 grit size. After paper polishing, the specimens were further finished by cloth polishing with 0.25- μm diamond paste. The etching was done by using Vilella's reagent (1 g picric acid + 100 ml ethanol + 5 ml HCL) to reveal the microstructure. The microstructural images were taken by using DMI 5000 M Light Optical Microscope (LOM). A FESEM was used to take the SEM (scanning electron microscope) images of the microstructures. The volume fraction of delta-ferrite was calculated using quantitative metallography (point count method) in ImageJ software. In these calculations, five optical microstructural images were used for each condition to ensure the reproducibility of the results.

The X-ray analysis was done by X-ray diffraction (XRD) patterns on X'Pert HighScore Plus software with PDF4 plugged in. These patterns were recorded by using the Rigaku Smartlab X-ray Diffractometer with CoK_α radiation (wavelength (λ) = 1.77 Å). The patterns were recorded for a 2θ range of 30° – 120° at the rate of $2^\circ/\text{min}$.

The hardness was measured on FIE VM50 Vickers Hardness Tester. The tests were performed at 10-kg load with 15-s dwell time. The specimens were prepared as per standard metallographic techniques before performing the tests. The average of the 10 readings along with the standard deviation has been reported. The micro-hardness of individual phases was measured by using UHL VMHT micro-hardness tester on a 50-g load and a dwell time of 15 s. For micro-hardness tests, the average of five readings for each phase along with standard deviation has been reported. A minimum gap of five times the diameter of the indenter between each indentation was ensured while performing the micro- and macro-hardness tests.

The tensile strength of as-received and processed specimens was characterized by conducting room temperature tensile tests on Tinius Olsen H25KS tensile testing machine. The miniature specimens (flat SS-3 type) were used for conducting the tensile tests. The geometry of the tensile specimen is shown in Fig. 3 [11, 19]. These tests were performed on 0.5 mm per minute cross-head speed. To maintain the accuracy, five specimens were tested and the average value has been reported.

The wear behavior was assessed by conducting sliding wear tests against a hardened EN31 steel disk on PIN ON DISC TRIBOTESTER TR-20E-PHM-250 (DUCOM). The pin samples of 6 mm diameter and 10 mm height were prepared for as-received and cyclically processed

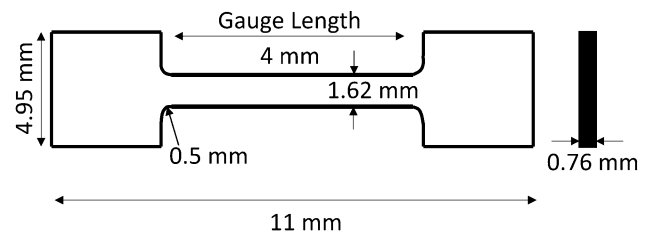


Fig. 3 The schematic geometry of flat SS-3 type miniature tensile specimen

specimens. The pin samples were polished by fine-grade emery papers to finish the surface. The surface roughness was measured by using Mitutoyo SJ-400 profilometer. The average R_a value of $0.22 \pm 0.04 \mu\text{m}$ was achieved after polishing. The tests were performed on 10 N, 20 N, 30 N loads with a sliding velocity of 1 m per second. Three specimens were tested for each condition and at each load. The wear behavior was recorded after the exposures of 1200 m, 2400 m, and 3600 m in each test. The disk and the samples were properly cleaned by acetone before and after each exposure. These tests were conducted in an air-conditioned room where 24°C temperature and 45% relative humidity were maintained. The worn surface was examined after 3600 meters of the test run in each case. The scanning electron microscope (SEM Zeiss EVO18[®]) was employed to take the digital images of worn surfaces.

3 Results and Discussion

3.1 Microstructure Examination

The optical microstructures of the as-received and cyclic heat-treated specimens are presented in Fig. 4. The optical microstructure of 13-4 ASR (Fig. 4a) consists of lath martensite and large colonies of delta-ferrite. Figure 4b, c shows the optical microstructure of 1000-2c and 1000-4c specimens, respectively. It can be seen that the microstructure of 1000-2c and 1000-4c consists of dissolved martensite and relatively smaller colonies of delta-ferrite. In the lath martensite morphology, the blocks are considered the most important parameter among the three levels because the block size is generally taken as the equivalent grain size [20, 21]. The blocks in the lath morphology are identified by the misorientation angle lesser than 10.53° [22]. Here, it is not easy to distinguish the blocks in the optical micrographs shown in Fig. 4. So, SEM micrographs were studied for a closer examination of the microstructures which are shown in Fig. 5. The SEM micrographs of 13-4 ASR and 1000-4c are shown in Fig. 5a, b, respectively. The dotted lines in Fig. 5a, b spectacle the approximate boundary of the blocks. A

Fig. 4 The optical microstructures illustrating the presence of lath martensite and colonies of delta-ferrite in: **a** 13-4 ASR, **b** 1000-2c, and **c** 1000-4c

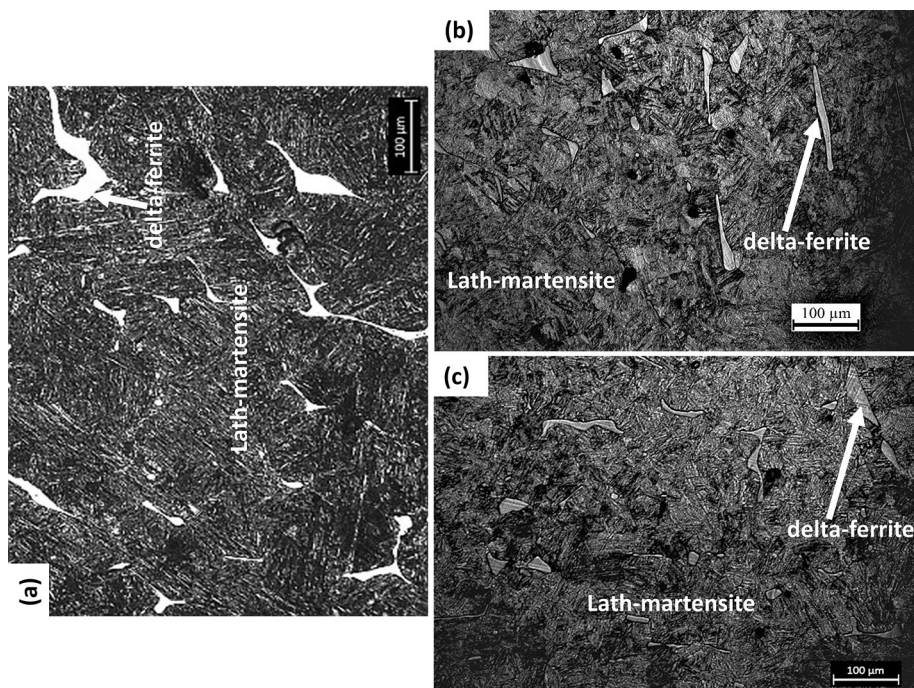
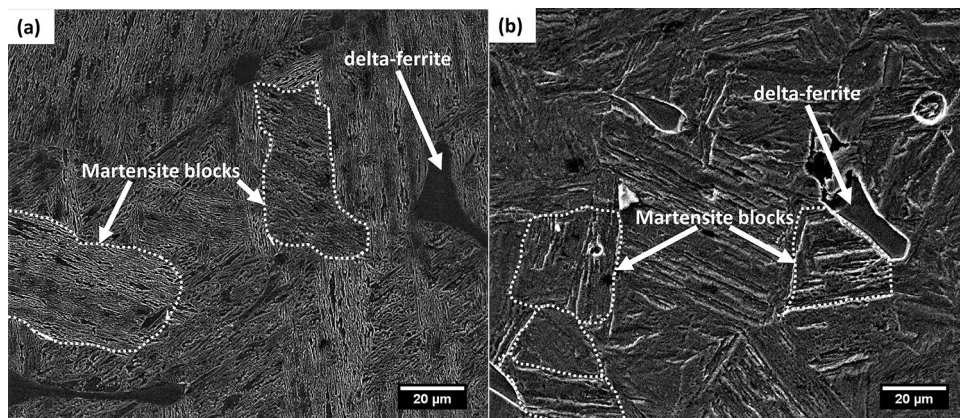


Fig. 5 The SEM micrographs illustrating the blocks of lath martensite and colonies of delta-ferrite in: **a** 13-4 ASR and **b** 1000-4c specimens



significant block refinement for the cyclic heat-treated specimen (1000-4c) can be visualized from the SEM micrographs (Fig. 5). This refinement is due to the disruptions in the parallelism of martensitic laths which is caused by the rapid and cyclic transformation of the alloy (13-4 MSS) between martensite (body-centered tetragonal, BCT) and austenite (face-centered cubic, FCC) [23–25]. These disruptions increase the densities of high angle boundaries within a martensite packet and thereby causes the refinements of martensite blocks [25]. The quantitative assessment of the block refinement has not been performed in this study.

Figure 6 shows the XRD spectra for both 13-4 ASR and cyclic heat-treated specimens. The X-ray analysis confirms the phases present in the optical micrographs. The XRD spectra of 13-4 ASR specimen comprise the peaks of

martensite (body-centered tetragonal, BCT), delta-ferrite (body-centered cubic, BCC), and retained austenite (face-centered cubic, FCC), whereas 1000-2c and 1000-4c specimen comprise the peaks of martensite (BCT), delta-ferrite (BCC) only. The peaks of retained austenite disappear from the cyclic heat-treated specimens. Also, it can be observed that the intensities of the delta-ferrite peaks in cyclic heat-treated specimens got reduced. This clearly indicates the reduction in volume fraction of delta-ferrite in cyclic heat-treated specimen. The peaks of martensite and delta-ferrite are overlapped in Fig. 6. This is due to the low carbon content in the current material. For low carbon content, the BCT structure approaches the BCC structure. The volume fractions of delta-ferrite and martensite calculated using quantitative metallography are presented in Table 1. In these calculations, the volume fraction of

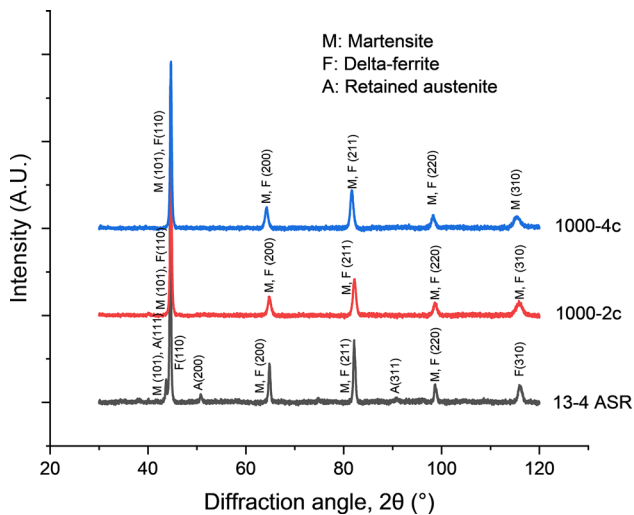


Fig. 6 X-ray diffractograms of as-received and cyclic heat-treated specimens

Table 1 Volume fractions of delta-ferrite in ASR and cyclic heat-treated specimens

	ASR	1000-2c	1000-4c
Volume fraction of δ -ferrite (%)	12.5 ± 0.2	6.7 ± 0.5	6.0 ± 0.3

retained austenite has been assumed to be zero because of its negligible amount. From Table 1, it can be seen that the amount of delta-ferrite is reduced from 12.5 to 6.0% and hence the amount of the martensite increases. This is a big achievement of this work because delta-ferrite is very soft and ductile due to lesser carbon solubility in delta-ferrite [21] and hence undesirable. Also, it is very difficult to remove delta-ferrite by conventional heat treatments [26]. The martensite is desirable here because of its high hardness. In addition to the reduction in delta-ferrite, a significant block refinement for the cyclic heat-treated specimens has also been observed.

3.2 Mechanical Properties

The amounts of delta-ferrite and martensite significantly influence the mechanical properties of the martensitic stainless steel [26]. Here, the mechanical properties are studied in terms of hardness and tensile properties. Figure 7 presents the variation of micro- and bulk hardness of 13-4 ASR and cyclic heat-treated specimens. It can be observed that a significant increase in microhardness of martensite and a slight decrease in micro-hardness of delta-ferrite is obtained due to the cyclic treatment. The microhardness of martensite is mainly controlled by the sizes of martensite blocks [20] and martensite laths [27] in martensitic steels. The size of blocks and laths has not been

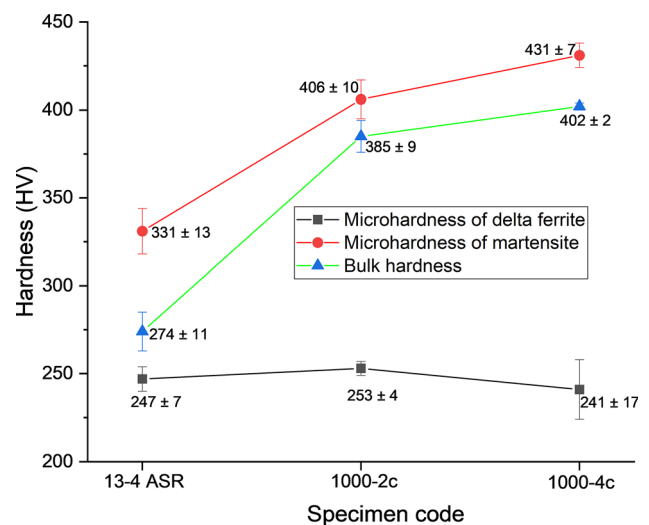


Fig. 7 Increased micro- and bulk hardness due to the cyclic heat treatment

assessed quantitatively in the current study. The visual inspection of the SEM micrographs in Fig. 5 confirms the refinement of martensite blocks. The increased number of block boundaries due to the refinement causes more hindrance to the motion of the dislocations across the block boundaries and thereby increases the hardness.

The volume fraction of delta-ferrite is much smaller as compared to the martensite counterpart in both the specimens (see Table 1). So, the bulk hardness is largely controlled by the martensite in each specimen. It can be seen from Fig. 7 that the bulk hardness of 1000-4c is much higher than the counterpart of 13-4 ASR. A 30% rise in microhardness of martensite and a 46% rise in bulk hardness have been achieved in 1000-4c as compared to 13-4 ASR specimen. The bulk hardness of 1000-2c specimen increases by 40% than the bulk hardness of 13-4 ASR. The bulk hardness of the martensitic stainless steels depends on the fractions of martensite and delta-ferrite [21], retained austenite [20]. In the present study, the cyclic heat treatment reduces the delta-ferrite and retained austenite and thereby increases the martensite content as shown in Table 1 and Figs. 4 and 5.

Table 2 presents the improvement in the tensile properties of the treated specimen as compared to the as-received condition. From Table 2, it is observed that a good improvement in the yield strength and ultimate tensile strength of the treated specimen is obtained. All the hardness controlling parameters influence the yield (YS) and ultimate tensile strength (UTS) of the present steel in a similar fashion. In the case of cyclic heat-treated specimen, these parameters favor the increased YS and UTS (see Table 2). The refined block size increases the strength as per classical Hall–Patch strengthening equation [28]. A

Table 2 Improved tensile properties (yield strength and ultimate tensile strength) due to CHT treatment

	As-received	1000-2c	1000-4c
Yield strength (MPa)	712 ± 20	1123 ± 10	1177 ± 11
Ultimate tensile strength (MPa)	897 ± 1	1210 ± 15	1269 ± 30
Ductility (%)	23.5 ± 1	21.9 ± 0.5	21.5 ± 0.5

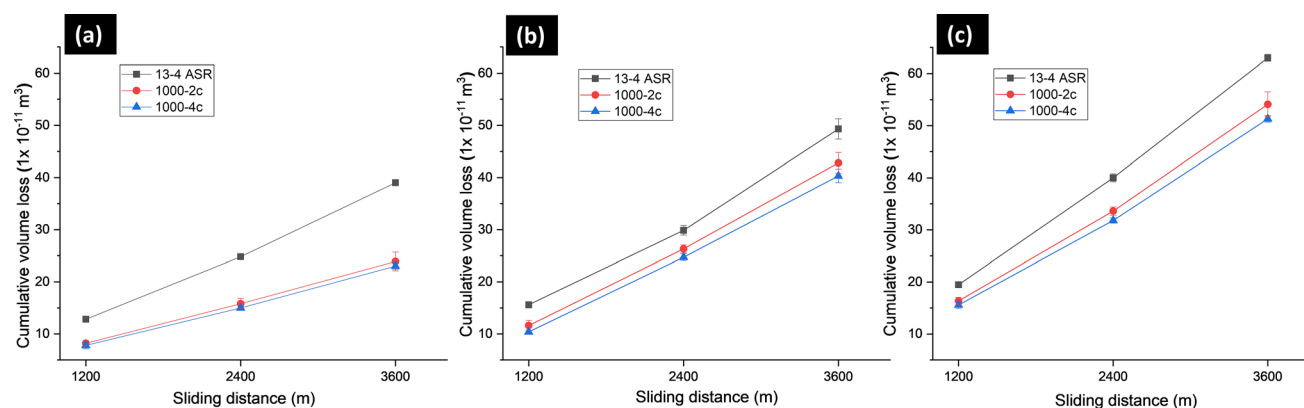
small reduction in ductility of cyclic heat-treated specimens is also observed as compared to the counterpart of 13-4 ASR specimen. This is due to the early plastic deformation of the specimen due to the reduced amount of delta-ferrite in cyclic heat-treated specimens. As mentioned earlier, delta-ferrite is soft and ductile [21]. The present cyclic treatment (CHT) increases the yield strength by 65% and the ultimate tensile strength by 41%. The 1000-4c specimen obtain the best combination of hardness (402 HV) and tensile properties (1177 MPa YS, 1269 MPa UTS, 21.5% ductility). This combination is better than conventional heat treatments [4–8] and other techniques [11] available in the literature. Also, this treatment has improved the mechanical properties without impairing the other properties.

3.3 Wear and Friction Characteristics

The wear behavior of ASR and cyclic heat-treated specimens is shown in Figs. 8 and 9. The variation of cumulative volume loss at different sliding distances of the wear test is shown in Fig. 8a for 10 N load, Fig. 8b for 20 N load, and Fig. 8c for 30 N load. The volume loss readings have been taken on the exposures of 1200 m, 2400 m, and 3600 m sliding distance in each run of the test. The sliding velocity is kept constant of 1 m/s. It can be observed that the cumulative volume loss increases with the sliding distance. For 13-4 ASR specimen, the volume loss is larger at

each load and continuously increases with the sliding distance as compared to the corresponding volume losses for cyclic heat-treated specimens. It can also be observed that the volume loss at 3600 m sliding distance is almost the double of the volume loss at 2400 m, particularly at higher loads. The wear rate calculated by volume loss per meter sliding distance (m^3/m) in each interval is shown in Fig. 9. The wear rate has been calculated for each load (Fig. 9a for 10 N load, Fig. 9b for 20 N load, and Fig. 9c for 30 N load) for all the cases. From the figure, it is observed that the wear rate remains almost similar throughout the sliding at 10 N for all the specimens. At 20 N, the wear rate decreases in the second interval for 13-4 ASR, while it increases continuously for cyclic heat-treated specimens. It continuously increases for all the specimens at 30 N load as shown in Fig. 9c. Cumulatively, the cyclic heat-treated specimens experience a lesser wear rate at each load and the wear rate increases with the increase in load for all the specimens. The 1000-4c specimen is found to be the most wear resistant among all studied in the present work.

The wear rate or volume loss increases when the sliding is done on higher loads (i.e., 10–30 N). This is due to the formation of an oxide layer at the interface of metal to metal contact at lower loads [29]. This layer acts as a barrier to the wearing away of the material. At higher load, the wear rate becomes severe due to the wearing away of the oxide layer. Also, as the sliding distance increases, the volume loss increases due to the oxidative-metallic wear.

**Fig. 8** The cumulative volume losses observed for 13-4 ASR and cyclic heat-treated specimens at: **a** 10 N load, **b** 20 N load, and **c** 30 N load

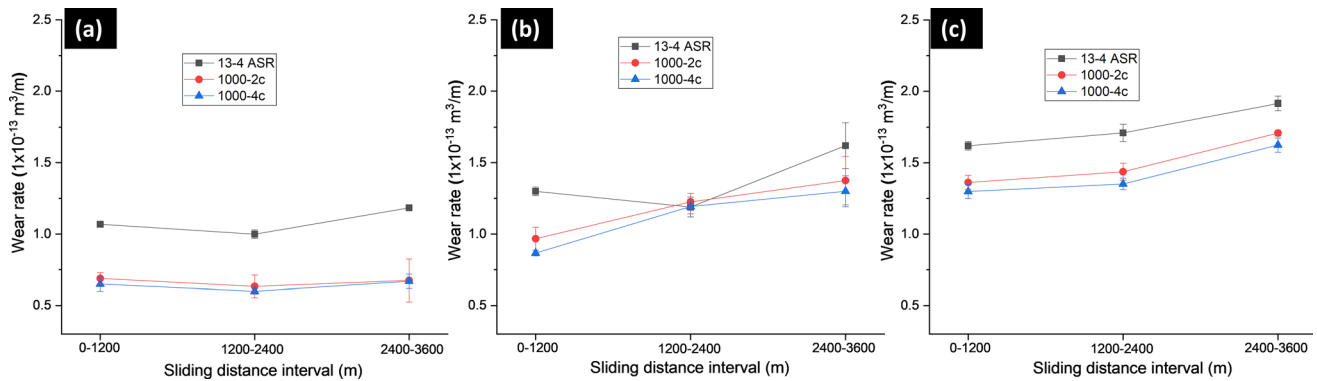


Fig. 9 The wear rate observed for 13-4 ASR and cyclic heat-treated specimens at: **a** 10 N load, **b** 20 N load, and **c** 30 N load

After the wear of this layer, the penetration of the asperities causes severe wear.

From Figs. 8 and 9, it is observed that the cyclic heat-treated specimens behave as higher wear-resistant material. This increased wear resistance is due to the improved mechanical properties of the treated specimen. Hardness is a major factor influencing the wear resistance of the material [30]. High hardness restricts the wearing of the material surface. Firstly, the asperities come into contact with the sliding disk. If the hardness of the asperities is higher, then the wearing of the surface will be lesser. For the treated material, the main content is hard martensite (94%) having microhardness of 431 HV which is far higher than the counterpart of ASR specimen (331 HV). Also, the bulk hardness is higher for 1000-4c specimen (402 HV) and 1000-2c specimen (385 HV) (see Fig. 6).

In addition to the hardness of the mated surface, the ultimate tensile strength also plays an important role in the wear behavior of the material. The wear of a surface occurs due to the deformation of the contact entities (i.e., asperities). The ultimate tensile strength indicates the strength required to deform a material. The asperities on the surface of the treated specimen are of higher UTS (deformation strength) which can be seen from Table 2. The deformation-resistant asperities undergo limited plastic deformation.

The friction behavior studied during the wear test is presented in Fig. 10. The variation of coefficient of friction (COF) during the first exposure (i.e., 1200 m) for ASR specimen at 10 N load is shown in Fig. 10a. It can be observed that the COF become stable after sliding for some distance. The COF become stable for each exposure of all the specimens in a similar fashion. The average COF values at different exposures calculated at each load for 13-4 ASR and 1000-4c specimens are shown in Fig. 10b. The COF at 10 N load is found to be the lowest for 1000-4c specimen, and its value at 10 N load become stable in other exposures for both cases (13-4 ASR and 1000-4c). It has been found to be slightly lower for the other two loads (i.e.,

20 N and 30 N) too as compared to the counterpart of ASR specimen. The reduced COF favor the minor surface deformation and reduced wear rates and the volume losses for the cyclic heat-treated specimens. It can also be observed that in the case of 20 N load, the COF decreases first and then increases for both the specimens. The COF at higher loads (30 N) increases continuously with the sliding distance. It can be concluded that the variation of COF values follow a different trend at each load. This friction behavior is in contrast with other researchers [31] which states the reduction of COF at higher loads except in the first interval at 30 N load.

3.4 Worn Surface

The worn surfaces have been studied to analyze the wear mechanism at different loads (low and high) and conditions (as-received and cyclic heat-treated specimens). Figure 11 demonstrates the effect of loads on wear mechanisms through SEM micrographs. Figure 11a presents the wear tracks of 13-4 ASR specimen at 10 N load. The small grooves indicate less penetration of asperities and lesser plastic deformation of the surface. Few minor craters also favor the less amount of volume loss. In addition to that, the oxide layer is also formed on some areas of the micrographs. Figure 11b represents the SEM micrographs of worn ASR specimen at a higher load of 30 N. At this much higher load, the oxide layer is worn away and it accelerates the volume loss from the surface. The deep grooves in Fig. 11b causes the plowing of the material and hence the plastic deformation. The coarse debris can also be observed on the micrograph which indicates that severe plastic deformation has occurred at this high load.

The previous sub-section has shown the increased wear resistance of the cyclic heat-treated specimen. The effects of cyclic treatment on wear tracks are shown in Fig. 12. Figure 12 shows the worn surface morphology of the 13-4 ASR (Fig. 12a) and 1000-2c (Fig. 12b), and 1000-4c

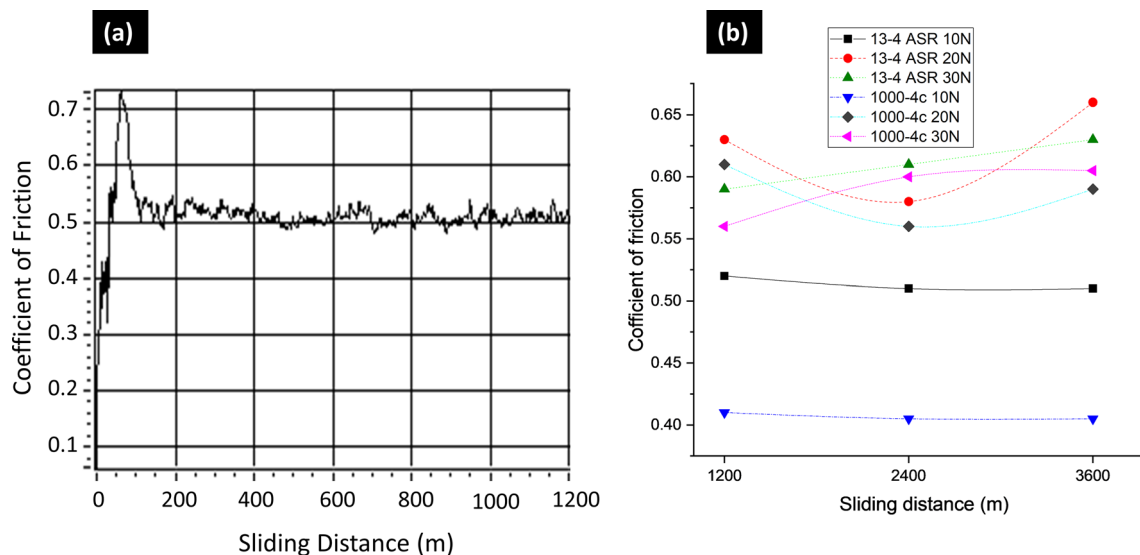
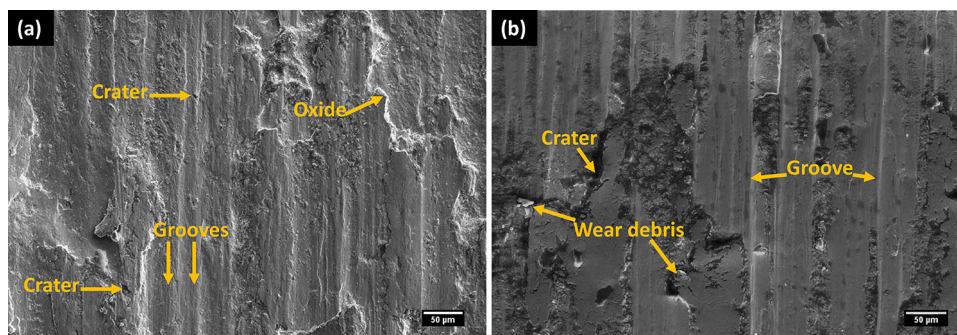


Fig. 10 The variation of coefficient of friction: **a** COF variation in the first exposure (1200 m) of 13-4 ASR at 10 N load, and **b** the average COF value at different exposures for 13-4 ASR and 1000-4c specimens

Fig. 11 The SEM wear tracks showing the wear mechanisms for 13-4 ASR worn specimens at **a** low load (10 N), and at **b** high load (30 N)



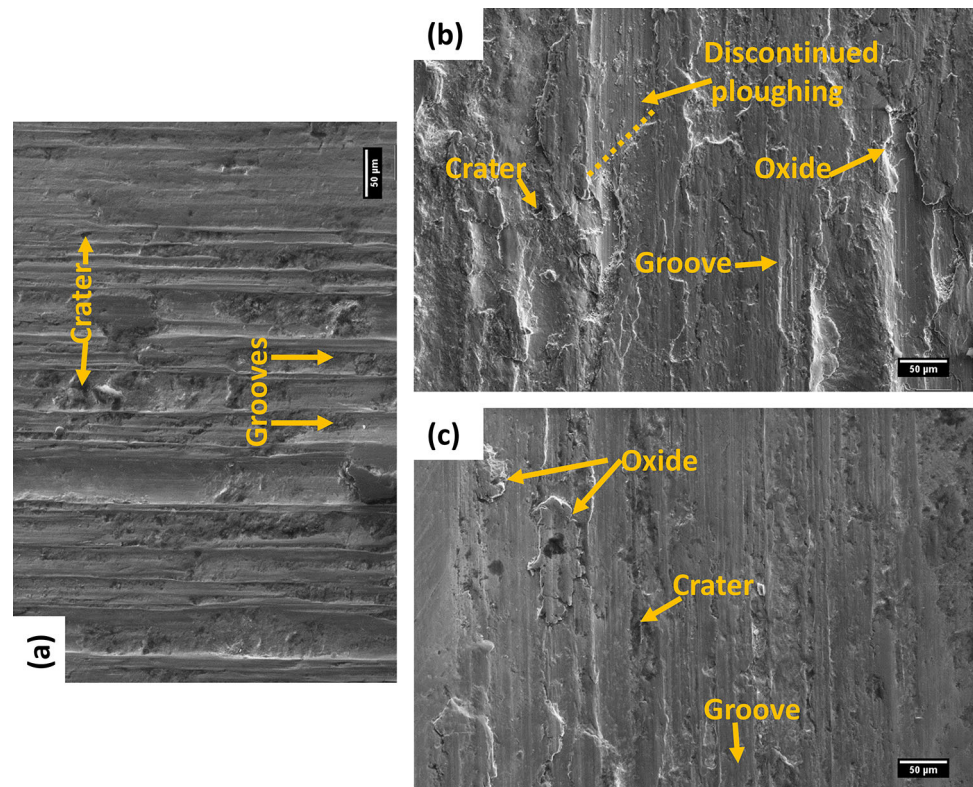
(Fig. 12c) after sliding of 3600 m distance at 30 N load. For as-received conditions, the large asperities penetration causes the formation of deep grooves and craters of a larger area. Hence, the higher wear rate and larger volume loss is encountered in the ASR specimen. The deep parallel grooves damage the surface by plow wear. However, very less number of craters are observed on the wear tracks of the cyclic heat-treated specimens. Also, the size of the craters is small. The depth of the grooves formed is also smaller, and the plowing is discontinuous in cyclic heat-treated specimens (1000-2c and 1000-4c). This is probably due to the higher hardness and reduced ductility of the cyclic heat-treated specimens. The higher hardness is responsible for the formation of hard oxides on the surfaces of cyclic heat-treated specimens. That is why, some oxide is still visible on the wear tracks of 1000-2c (Fig. 12b) and 1000-4c (Fig. 12c) specimens, while it wears away for the as-received specimen. The presence of shallow craters and less deep grooves in the case of 1000-4c verifies the results of the limited wear rate and volume losses.

4 Conclusions

A cyclic heat treatment was performed on 13-4 MSS in order to improve its mechanical properties and wear characteristics. The wear behavior of as-received and treated specimens was studied by conducting sliding wear (pin-on-disk) test, and the following conclusions could be made:

- The cyclic heat treatment refined the martensite blocks, reduced the amounts of delta-ferrite and retained austenite from the 13-4 ASR which significantly improved the hardness and tensile properties for cyclic heat-treated specimens. The 1000-4c specimen obtain the best combination of hardness (402 HV), yield strength (1177 MPa), ultimate tensile strength (1269 MPa), and ductility (21.5%).
- The improved hardness and the ultimate tensile strength (UTS) of the cyclic heat-treated specimens decreased the volume loss and the wear rate. The specimen having

Fig. 12 The SEM wear tracks showing the effect of cyclic heat treatment on wear mechanisms in: **a** 13-4 ASR, **b** 1000-2c, and **c** 1000-4c specimen



4 cycles of cyclic heat treatment (1000-4c) possessed the higher wear resistance than the specimen having 2 cycles (1000-2c) due to its superior mechanical properties.

- The worn surface morphology consisted of small and deep grooves and craters causing plowing wear mechanism for both the as-received and cyclic heat-treated specimens. The reduced ductility and the higher hardness and UTS caused the discontinuous plowing in the cyclic heat-treated specimens.

The cyclic heat treatment improved the mechanical properties and wear behavior of 13-4 MSS in an effective way. This achievement further motivated us to study the erosive wear behavior of the current steel with the current treatment.

References

1. Prakash G, and Nath S K, *J Mater Eng Perform* **27** (2018) 3206. <https://doi.org/10.1007/s11665-018-3424-5>.
2. Vadiraj A, Kamaraj M, and Sreenivasan VS, *Surf Eng* **28** (2012) 192. <https://doi.org/10.1179/1743294411y.0000000003>.
3. Goyal V, Sharma S K, and Kumar B V M, *Mater Today Proc* **2** (2015) 1082. <https://doi.org/10.1016/j.matpr.2015.07.013>.
4. Amarendra H J, Kalhan P, Chaudhari G P, Nath S K, and Kumar S, *Mater Sci Forum* **710** (2012) 500. <https://doi.org/10.4028/www.scientific.net/msf.710.500>.
5. Akhiate, A., Braud, E., Thibault, D., & Brochu, M. Carbon content and heat treatment effects on microstructures and mechanical properties of 13%Cr–4%Ni martensitic stainless steel. COM 2014, Conference of Metallurgist (2014: Vancouver). Vancouver, Canada.
6. Bashu S A, Singh K, and Rawat M S, *Mater Sci Eng A* **127** (1990) 7. [https://doi.org/10.1016/0921-5093\(90\)90184-5](https://doi.org/10.1016/0921-5093(90)90184-5).
7. De Sanctis M, Lovicu G, Buccioni M, Donato A, Richetta M, and Varone A, *Metals (Basel)* (2017). <https://doi.org/10.3390/met7090351>.
8. Zhang S, Wang P, Li D, and Li Y, *Mater Des* **84** (2015) 385. <https://doi.org/10.1016/j.matdes.2015.06.143>.
9. Severo F S, Scheuer C J, Cardoso R P, and Brunatto S F, *Wear* **428–429** (2019) 162. <https://doi.org/10.1016/j.wear.2019.03.009>.
10. Grewal H S, Arora H S, Singh H, and Agrawal A, *Appl Surf Sci* **268** (2013) 547. <https://doi.org/10.1016/j.apsusc.2013.01.006>.
11. Kishor B, Chaudhari G P, and Nath S K, *Tribol Int* **93** (2016) 50. <https://doi.org/10.1016/j.triboint.2015.08.048>.
12. Kishor B, Chaudhari G P, and Nath S K, *Wear* **319** (2014) 150. <https://doi.org/10.1016/j.wear.2014.07.024>.
13. Mann B S, and Arya V, *Wear* **249** (2001) 354. [https://doi.org/10.1016/s0043-1648\(01\)00537-3](https://doi.org/10.1016/s0043-1648(01)00537-3).
14. Grewal H S, Agrawal A, and Singh H, *Tribol Int* **66** (2013) 296. <https://doi.org/10.1016/j.triboint.2013.06.010>.
15. Nath G, and Kumar S, *Metallogr Microstruct Anal* **7** (2018) 133. <https://doi.org/10.1007/s13632-018-0426-5>.
16. Mishra S, Mishra A, Show B K, and Maity J, *Mater Sci Eng A* **688** (2017) 262. <https://doi.org/10.1016/j.msea.2017.02.003>.

17. Mishra A, and Maity J, *Mater Sci Eng A* **646** (2015) 169. <https://doi.org/10.1016/j.msea.2015.08.018>.
18. Ravi Kumar B, Sharma S, Kashyap B P, and Prabhu N, *Mater Des* **68** (2015) 63. <https://doi.org/10.1016/j.matdes.2014.12.014>.
19. Kishor B, Chaudhari G P, and Nath S K, *Tribol Int* **119** (2018) 411. <https://doi.org/10.1016/j.triboint.2017.11.025>.
20. Morito S, Yoshida H, Maki T, and Huang X, *Mater Sci Eng A* **440** (2006) 237. <https://doi.org/10.1016/j.msea.2005.12.048>.
21. Galindo-Nava E I, and Rivera-Díaz-del-Castillo P E, *Acta Mater* **98** (2015) 81. <https://doi.org/10.1016/j.actamat.2015.07.018>.
22. Kitahara H, Ueji R, Tsuji N, and Minamino Y, *Acta Mater* **54** (2006) 1279. <https://doi.org/10.1016/j.actamat.2005.11.001>.
23. Hidalgo J, and Santofimia M J, *Metall Mater Trans A Phys Metall Mater Sci* **47** (2016) 5288. <https://doi.org/10.1007/s11661-016-3525-4>.
24. Kim H J, Kim Y H, and Morris J W, *ISIJ Int* **38** (1998) 1277. <https://doi.org/10.2355/isijinternational.38.1277>.
25. Nasiri Z, Ghaemifar S, Naghizadeh M, and Mirzadeh H, *Met Mater Int* (2020). <https://doi.org/10.1007/s12540-020-00700-1>.
26. Wang P, Lu S P, Xiao N M, Li D Z, and Li Y Y, *Mater Sci Eng A* **527** (2010) 3210. <https://doi.org/10.1016/j.msea.2010.01.085>.
27. Wang X D, Zhong N, Rong Y H, Hsu T Y, and Wang L, *J Mater Res* **24** (2009) 260. <https://doi.org/10.1557/jmr.2009.0029>.
28. Zhang C, Wang Q, Ren J, Li R, Wang M, Zhang F, and Sun K, *Mater Sci Eng A* **534** (2012) 339. <https://doi.org/10.1016/j.msea.2011.11.078>.
29. Mohan S, Prakash V, and Pathak J P, *Wear* **252** (2002) 16. [https://doi.org/10.1016/s0043-1648\(01\)00834-1](https://doi.org/10.1016/s0043-1648(01)00834-1).
30. Ho J W, Noyan C, Cohen J B, Khanna V D, and Eliezer Z, *Wear* **84** (1983) 183. [https://doi.org/10.1016/0043-1648\(83\)90263-6](https://doi.org/10.1016/0043-1648(83)90263-6).
31. Rakesh Kumar G, and Suresh Kumar Reddy N, *Mater Today Proc* (2020). <https://doi.org/10.1016/j.matpr.2020.01.509>.

Publisher's Note Springer Nature remains neutral with regard to jurisdictional claims in published maps and institutional affiliations.